Enhancing Punching Shear Capacity of Flat Slabs with Hidden Capitals made of Strain Hardening Cementitious composite (SHCC)

Mahmoud Ahmed Abdelaziz, Nesreen Kassem, Mohamed Hussien

Enhancing Punching Shear Capacity of Flat Slabs with Hidden Capitals made of Strain Hardening Cementitious composite (SHCC)

Mahmoud Ahmed Abdelaziz [1], Nesreen A. Kassem[2], Mohamed A Hussien[3]

[1] Structural Engineering Department, Faculty of Engineering, Tanta University, Tanta, Egypt – mahmoud.abdelaziz@f-eng.tanta.edu.eg
[2] Professor of reinforced concrete structures-Structural Engineering Department, Faculty of Engineering Tanta University, Tanta, Egypt – nesreen.kassem@f-eng.tanta.edu.eg
[3] Professor of reinforced concrete structures, Structural Engineering Department, Faculty of Engineering Tanta University, Tanta, Egypt – mohamed.hussein@f-eng.tanta.edu.eg

Abstract-This paper focuses on studding the effect of using hidden capitals made of strain hardening cementitious composite (SHCC) to improve the punching shear resistance at slab-column connections. However, due to its the high cost, its use is often limited to the support zone. Ten 160 mm thick slabs with identical reinforcement and geometry were constructed in this investigation. Two control specimens, one loaded at the center of the column and the second loaded with eccentricity of 100mm. The other eight specimens were strengthened with SHCC hidden capitals to study the effect of the hidden capital's thickness, area, fiber content ratio in the SHCC, using drop, and load eccentricity on the punching shear behavior. The results showed that, the use of SHCC hidden capitals can effectively improve the cracking behavior and mode of failure. Due to the decrease in the severity of the crack inclination, the formation of cracks at tension side occurred within a larger radius than in the control specimen. The results showed also that, the capacity increased by 7%, 14%, and 22% as the thickness of the SHCC layer increased by 0.25, 0.5, and 0.75 times the slab thickness. Whereas the capacity increased by 5%, 14%, and 15%, with a corresponding increase in the extension of the SHCC layer by 0.5, 1.0, and 1.5 the slab depth. Also, the capacity increase by 14%, and 25.2%, as the fiber content in the SHCC layer increased from 1% to 2%. Corresponding increase in the capacity by 14% and 34.8%, by using drop part of one third the thickness of the SHCC layer outside the section by 0.0 and 0.25 slab thickness. The various parameters showed also a significant decrease in deflection, compression strains, tension strains, and increase flexural stiffness and ductility. Comparison with various world codes showed that the Egyptian code calculations involve a high degree of accuracy, less conservative, and are closest to the results of laboratory tests.

Keywords-Punching strength, Engineering cementitious composite, slab-column, connections, Flat plate.

I- INTRODUCTION

Flat slab systems are one of the most common structural options because they provide for greater flexibility in organizing space within structures, and they do not necessitate the storey height to be increased in order to preserve the needed useable area, as is the case of solid slabs. Also, they easier to implement formwork, and faster in construction time [1]–[5]. Flat slabs must be built to withstand bending moments as well as punching shear stresses. A rapid failure that results in the column punching through the slab is the usual failure mode of flat slabs owing to punching shear, Fig.

1. This sort of failure is one of the most important factors to consider when estimating the thickness of flat slabs or the column contact area at the slab-column junction[2], [6]. The self-weight of flat slabs is a significant engineering difficulty since employing thinner slabs lowers the increase in bending forces while increasing the danger of critical punching shear. At lesser slab thicknesses, reinforcing the connection may not be an ambitious approach to resist punching shear [6]–[8].

There have been many attempts to increase the punching shear capacity of slab-column connections for small thicknesses without using reinforcement. An article discusses the need for investigating parameters influencing the punching strength through analytical or experimental studies for flat slabs had drops, and columns with capitals [9]. The results suggest that intermediate and corner column connections are the governing criteria for prescribing drift limits for flat plate systems in seismic zones. Shear capitals or drop panels can be used to increase the punching shear strength of slab-column connections. Another research investigates the effectiveness of shear capitals and drop panels in increasing punching shear resistance of slab-column connections through experiments and finite element analysis [10]. The study finds that shear capitals may not be reliable in increasing punching shear resistance, and the ACI design criteria overestimates their strength. The indiscriminate use of shear capitals can lead to unsafe conditions when subjected to high moment transfer. An experimental study on hollow floor slab-column-reinforced connections, which are improved by installing a locally solid zone of the slab around the column and hidden beam in the floor [11]. The results showed that the connections had double failure characteristics of punching shear and flexural failure, with flexural failure being the main mode due to the hidden beam. The connections with punching components had higher initial stiffness and loading capacity than those without, with welding section steel cross bridging being more effective in improving punching-shear capacity than bent-up steel bars.

Manufacturing a portion of the flat slab with high-performance concrete or morters as hidden capitals improves the connection's performance in resisting punching shear, as it provides better resistance and the presence of fibers can help limit crack widening, acting as a bridge for loads even during fine cracking. By using this technique in resisting punching

shear, there are two conceivable failure scenarios, as indicated in Fig. 1, depending on the size of the capital and the relative strengths of the concretes involved. In the first instance, a diagonal fracture occurs on the column's edge and penetrates through the capital (Fig. 1a). The strength of both concretes determines the punching shear capacity. The diagonal fracture arises outside the capital in the second scenario, and the load capacity is regulated by the weaker concrete (Fig. 1b). This failure mechanism is similar to that seen in shear reinforced slabs, when failure occurs outside the reinforced area. This method of increasing the punching shear resistance of flat slabs made of lightweight aggregate concrete by using hidden steel fibre reinforced capitals was investigated [12], [13] . The research found that the addition of steel fibres to concrete has been shown to increase punching shear resistance and ductility. A paper provides an analysis of existing technical solutions for preventing punching shear failure in flat slabs [14]. The study analyzes the control extent, columns with capitals, and various examples of eccentricity at punching shear. It also describes punching reinforcements and their inappropriate use and provides a comparative analysis of contemporary devices for punching shear prevention.

Engineered cementitious composites are micromechanically engineered composite materials mixed with random short fibres that have a fibre volume fraction of less than 2-3% and exhibit different cracking behaviors as well as tensile strain hardening properties [15]. The strain hardening cementitious composite (SHCC) has various pros. Their maximum tensile strain is up to 5%, which is substantially higher than the maximum tensile strain of typical concrete [16]. In contrast to regular RC beams, many small cracks are anticipated to occur on the tensile side of RC members when SHCC is applied [17]. The sparsely spaced small cracks will effectively disperse stress throughout the FRP jacket and reduce crack-induced stress concentration. Due to these qualities, SHCC is an excellent repair material [18].

The ability to adjust crack width, high deformation, high damage tolerance, energy absorption, delamination resistance, shear load resistance, and high durability are just a few of the advantageous traits of SHCC that researchers have found to be useful in reinforcing or repairing structures. For instance, Lim and Li [19] discovered that SHCC were successful at trapping interface fractures, hence eradicating frequent failure modes in a SHCC/concrete strengthening system, such as early or surface spalling, and extending the system's service life. According to Suthiwarapirak et al. [20], SHCC has a substantially higher capacity for fatigue resistance than conventional repairing materials. SHCC can also reduce shrinkage crack width and are freeze-thaw resistant [21].

In recent years, numerous studies on the use of SHCC to increase structural responsiveness have been carried out, including the repair or improvement of the performance of buildings or bridges [22], [23]. Some researchers have been applied in the field of flat slabs to enhance the shear strength. Punching shear behavior of slabs made from different types of concrete internally reinforced with SHCC-filled steel tubes was studied [24]. Internally unreinforced slabs made of

UHPFC and SHCC avoided punching shear failure and collapsed in a ductile bending pattern was concluded.

Despite the fact that the offered topic has received substantial treatment in the literature, few studies are dedicated to the use of SHCC to improve the punching shear resistance of flat slabs. The study's primary goal was to push the present to give recommendations in the use of hidden capitals of SHCC. This would allow the maximum efficacy of the SHCC hidden capitals to be determined.
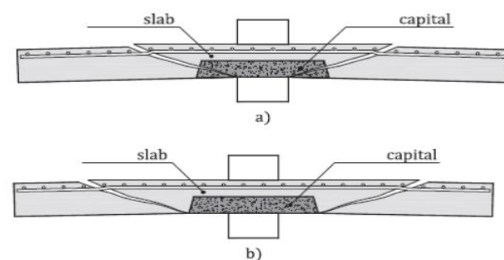

Figure 1. Punching shear failure.

Figure 2. Possible punching shear modes of failure for flat slabs with hidden capitals.

II- HIGHLIGHTS

This research highlights the effect of some parameters of using SHCC hidden capitals on the punching shear capacity of slab-column connections. The study considers variables such as the hidden capital's thickness, hidden capital's area, fiber content ratio in the SHCC, and using drop on the punching shear behavior. The research also examines the effect of transferred moments from the flat slab to the column by applying eccentric load in the test. The results were presented in the form of the effect of variables on the crack pattern, the collapse mechanism, load-deflection, load capacity, deformations and strains in concrete and steel, and finally ductility.
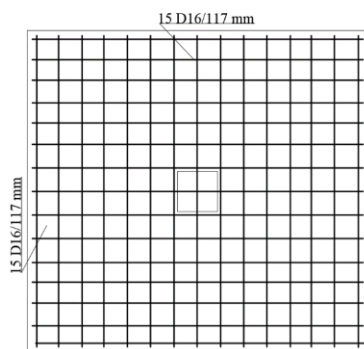
III- TEST PROGRAM

A. Specimen selection and detailing

A specimen was selected to represent a portion of the slab around a column of a flat slab at regions of contraflexure points (zero moments) in both directions. Through the analysis of a flat slab with multiple bays of fixed dimensions in both directions with a length of 4.00 meters, it was found that the contraflexure points are located at a distance of 0.4 from the bay length, which is 1.60 meters. Therefore, a flat slab with dimensions of 1.7 meters by 1.7 meters was chosen to provide a span length of 1.60 meters, and a minimum thickness of 160 mm was selected to

82

correspond with the basic assumption of the study. The punching shear capacity of the slab was somewhat lower than the bending capacity to ensure a punching shear failure, despite being designed in compliance with the design code for concrete structures [25]–[28]. So, a column sections with dimensions of 200 mm × 200 mm and a height of 200 mm extended in one direction of the slab to form the column-slab connection. All slabs were reinforced with tensile reinforcement in both directions, using 9D16/m@117mm, and compression reinforcement only in the column region in both directions, with 3D12 mm to ensure good connection between the capital area and the slabs. The placement of compression reinforcement was neglected in the other parts of the slab. The presence of compression reinforcement increases slightly the shear strength of slabs [29]. The column was reinforced using 4D12 mm, bar at every corner and two stirrups were placed throughout the height of the column using 8mm diameter bars. Additional stirrups were also placed in the eccentric loading slabs. The slab S1 was used as a control slab. Fig. 3 shows dimensions, tension, compression reinforcements detailing and cross section of the control slab S_1 (unit: mm).
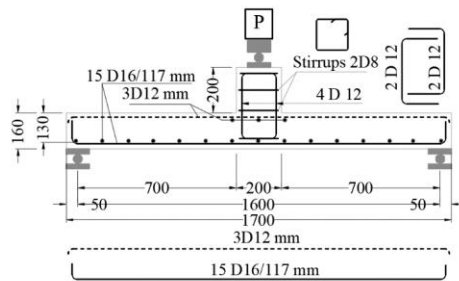
(a) Cross section elevation

(b) Main tension reinforcement
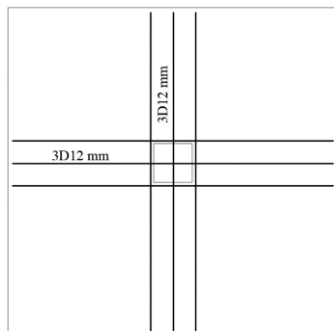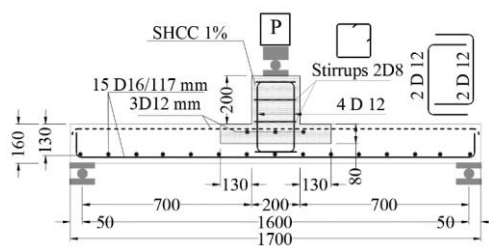

(c) Compression reinforcement

Figure 3. Dimensions and reinforcement details of control slab S1.

B. Test program

An experimental program was designed consisting of ten slabs, each representing a portion of the connection area between the flat slab and the column representing the area between contraflexure points. Several variables were studied in this experimental program, including the effect of the thickness of the hidden capitals, the effect of its surface area, the effect of varying the fiber volume size within the SHCC mixture, the effect of having a protruding part of the capital outside the slab (drop part) and finally, effect of load eccentricity by 100 mm in the behavior unstrengthen and strengthed slabs. The table 1 represents a summary of different parameters studied for reinforced concrete flat slabs with capital. The slabs are labelled as S1 to S10, with S1 and S9 serving as the control, while SHCC hidden capital was cast in the remaining slabs to improve the connection area. Slabs S2, S3 and S4 have a capital thickness of 120, 80, and 40 mm respectively and an end-of-capital distance of 130 mm from the column face. Fig. 4 shows dimensions, tension, compression reinforcements detailing and cross section of the slab S_3 (unit: mm). Slab S5 and S6 have the same capital thickness as S3, but a different end-of-capital distance from column face of 65, 195 mm respectively. Slab S7 has the same parameters as S3, but with a different fiber content in SHCC (2%). Slab S8 has the same parameters as S3, but with a different hidden capital location where in S3 120 mm thickness hidden capital has been replaced inside the slab but in S8, 40mm is located external, see Fig. 5a. S9 has the same parameters as S1 but the applied load was eccentric by 100 mm. S10 has the same load eccentricity as S9, but it appears to be related to the thickness, area, fiber volume and location of the hidden capital as S3. Fig. 5b shows dimensions, tension, compression reinforcements detailing on cross section of the slab S_{10} (unit: mm)

Table 1. Experimental test matrix

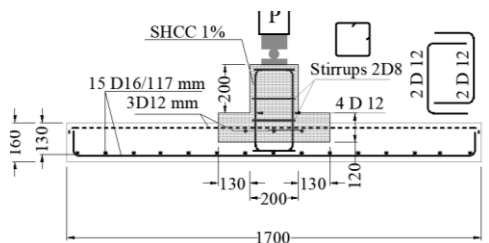| Slab	Capital thickness. (mm)	End of capital distance from column face (mm)	Fiber content	Capital Part placed outside the slab (mm)	Load eccentricity (mm)
S1	---	---	---	---	---
S2	120	130	1%	---	---
S3	80	130	1%	---	---
S4	40	130	1%	---	---
S5	80	65	1%	---	---
S6	80	195	1%	---	---
S7	80	130	2%	---	---
S8	80	130	1%	40	---
S9	---	---	---	---	100
S10	80	130	1%	---	100

(a) Cross section elevation
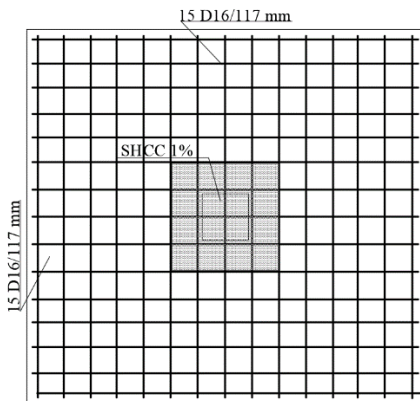
(b) Main tension reinforcement

Figure 4. Cross-section, dimensions, and reinforcement of S3.

(a) Cross-section, dimensions, and reinforcement of S8
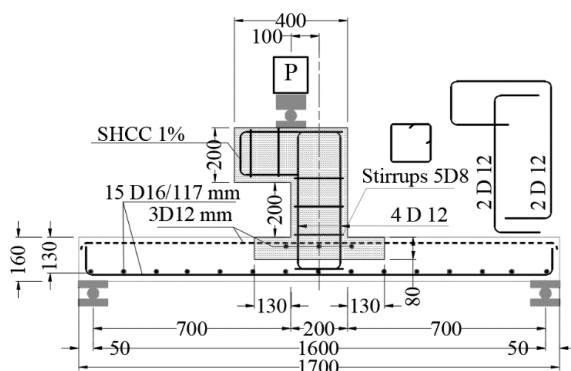
(b) Cross-section, dimensions, and reinforcement of S10

Figure 5. Cross-section, dimensions, and reinforcement of S8 and S10.

C. *Material properties*

To ensure that the concrete strength was consistent across all tested slabs, the same patch of ready-mixed concrete was used. The mixture contained ordinary Portland cement 42.5R

and table 2 shows the mix characteristics. The fine aggregates were cleaned river sand, with a density of 2650 kg/m³, while the coarse aggregates were made of limestone with a density of 2700 kg/m³ and a nominal maximum size of 20 mm. Standard cylinders with a height of 300 mm and diameter of 150 mm were used for compression tests in accordance with ASTM C39/C39M, and on the day of testing, the mean cylinder compressive strength (f'c) was 23.6 MPa (cubic compressive strength is 29.5 MPa). The true tensile strength was determined through Brazilian tensile testing on three cylinders, which had a mean tensile strength of 2.65 MPa at the time of testing.

Table 2 provides a list of the mix characteristics of SHCC, which contained ordinary Portland cement, fine silica sand, silica fume, polypropylene fibers, water, and superplasticizers. Fly ash and regular Portland cement were used as a binder. The flowability of the SHCC binder was improved by using a high range water reducer. The PE fibers had a diameter of 25 μm and length 12 mm and its properties are listed in table 3. Tensile and compressive tests were conducted on SHCC samples, with the tensile tests conducted on large size specimens to avoid size influence Li et al and Kunieda et al [16], [18]. The SHCC had an average first-cracking strength of 3.11 MPa and an average ultimate tensile strength of 6.71 MPa and 7.1 for 1% and 2% fiber content respectively. The average compressive strength of the tested specimens was 60.74 and 70.26 MPa for 1% and 2% fiber content respectively.

Two types of reinforcing steel were used for the tested slabs: grade 240/350 (N.M.S) plain round bars with a nominal diameter of 8 mm, and grade 400/600 (H.T.S) ribbed bars with a nominal diameter of 12 and 16 mm. Tensile tests were conducted on three standard specimens for each diameter, and the average yield and ultimate strengths, as well as the typical elastic modulus, are provided in Table 4.

The bond between the healing material and the substrate concrete is important. Slant shear tests were conducted on three cylindrical specimens in accordance with ASTM C882-99. The first half of the cylinder was cast using the concrete mixture used in the tested beams. The contact surface was roughened, and the concrete base was painted with epoxy resin before being covered with SHCC material. A structural resin epoxy (Kemapoxy 103) was used with an initial and final setting time of 15 and 60 minutes, respectively, and a density of 1.10±0.02 kg/L. After 28 days, the samples underwent compression tests and had an average slant shear strength of 16.85 MPa, with splitting failure occurring in the loading direction without sliding.

Table 2. Mix proportions of materials (kg/m3) for cubic meter

Mix	Water-to-binder ratio	Water	Super plasticizers	Fibres (volumetric ratio)	Silica fume	Coarse aggregate	Sand	Cement
NSC	0.5	175	-	-	-	1249	515	350
ECC 1.0%	0.2	312.1	31.6	8.1 (1.0%)	237	-	157.9	1342

ECC 2%	0.2	312.1	31.6	16.2 (2%)	236.7	-	157.7	1342

Table 3. Properties of PP fibres

Fiber	Diameter *df* (µm)	Length *Lf* (mm)	Aspect ratio *Lf/df*	Experiment al strength	Nominal Young's	Elongation at breakage	Specific gravity	Oil coating (%)	Melting point (°C)
PP Fiber	25	12	720	2900	116	2.42	0.97	/	150

Table 4. Steel reinforcement's characteristics

Diameter, mm	Yield strength, (MPa)	Ultimate strength, (MPa)	ε_y	ε_u	Es (x10^5 N/mm²)
8	274	365	0.00134	0.178	2.05
12	528	723	0.00256	0.132	2.05
16	534	727	0.00262	0. 138	2.05

D. Fabrication and preparation of test slab

The following is a summary of the sequence of operations for the construction of the slabs with SHCC hidden capitals:

1. The external formwork, then the bottom primary reinforcement was installed.
2. A mold-shaped capital was set, and holes in the mold were bored to allow the secondary reinforcement to pass through.
3. To maintain a sufficient effective depth, the three bars of the secondary reinforcement was installed, and spacer bars were employed near the slab edges.
4. Before casting the NSC concrete, these holes in the mold were filled, Fig. 6a and strain gages were paste in the existed locations at slab center and at d/2 from column face.
5. Using hand scoops, the volume between the external formwork and the mold was filled with NSC concrete and mechanically compacted with a poker vibrator, Fig. 6b.
6. After two days, the mold and exterior formwork were removed, and a column portion of the formwork was installed.
7. The concrete foundation was coated with epoxy resin after the contact surface was roughened.
8. Before covering with SHCC material, the work area was completely cleansed of any concrete residues.
9. SHCC was used to cast the column and hidden capital. The SHCC was mechanically crushed during installation using a rod vibrator, Fig. 6c.
10. The slabs were cured for about 10 days by spraying with water and covered with foil. The specimens were then unmolded and kept in the laboratory until the test day arrived.

The use of several types of concrete with differing casting intervals created a difficulty, but the building process was meticulously planned and carried out to assure the quality and integrity of the slabs with hidden capitals.

(a) Installation of reinforcing meshes inside the formwork and mold

(b) Casting of normal strength concrete

(c) Casting and curing of SHCC hidden capitals and the column

Figure 6. Fabrication and preparation of test slabs.

E. Loading program and instrumentations

Fig. 7 depicts the test equipment utilized in this experimental work. The test setup involved placing each of the slab on supports at the outer edges, where each edge was supported by a steel plate with a width of 50 mm and thickness of 10 mm. These plates, in turn, were supported by a bar with a diameter of 25 mm, which was supported by steel I-beams no. 20. In order to get the load-deformation curves under a monotonically increasing load till failure, the load was applied through a hydraulic jack with a maximum capacity of 1500 kN and the load measured from load cell attached to the load cell. The initial loading rate was 5.0 kN/s, however it dropped to 2.00 kN/s after yielding. There are eight LVDTs (linear variable differential transducers) attached to the specimens. four of them were mounted to measure vertical deformations: two at midspan, and two at the center of the supports. To calculate the tension and compression strains, two LVDTs are attached at the top of the slab at d/2 from the column face to get the compression strain. Another two LVDTs are attached at the bottom of the slab at d/2 from the column face to get the tension strain. Another three strain gages are mounted on the steel surface at various location to get the steel strains. The loads, displacements, and deformations were recorded using

an automated data accession system connected to a laptop through a USB link. To measure the crack width of the beam during loading, a second crack width calibrated tool was used. The load was raised and then halted at particular points to illustrate the fracture propagation. Full fracture patterns were supplied at the end of the test. When the load fell due to logical failure of the slab, the test was terminated.

(a) Instrumentation at upper surface
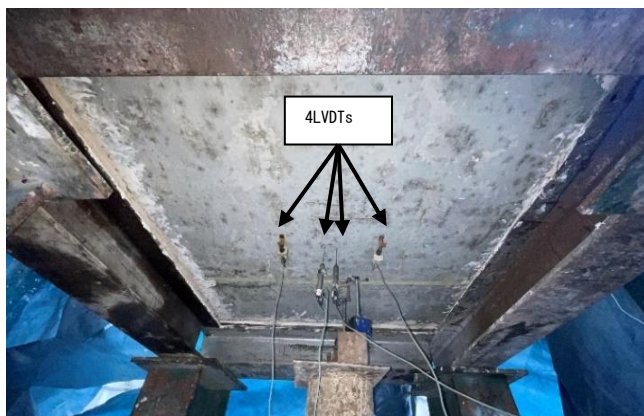
(b) Instrumentation at lower surface

Figure 7. Test setup.

IV- EXPERIMENTAL RESULTS

Table 5 contains a summary of the most important laboratory results, flexural cracking load, deflection at cracking load, ultimate load capacity, deflection at ultimate load, maximum compression strain, maximum tension strain, and Ductility.

Table 5. Experimental results

Slab	Flexural cracking load Pcr (kN)	Deflection at cracking load Δcr (mm)	Ultimate load capacity Pu (kN)	Deflection at ultimate load Δu (mm)	Maximum compression strain εcu (micro	Maximum tension strain εsu (micro strain)	Ductility (kN.m)
S1	112	0.812	459	10.62	2740	2046	2988
S2	118	0.800	562	11.68	3211	2544	3885
S3	115	0.802	523	11.65	2987	2311	3658
S4	113	0.800	493	11.22	2752	2214	3365
S5	113	0.800	482	11.19	2238	2187	3311
S6	115	0.803	530	11.47	2407	2292	3680
S7	116	0.750	575	14.01	2925	2612	5063
S8	122	0.775	660	13.93	2231	2242	5538
S9	105	0.820	430	10.57	2720	2036	2815
S10	108	0.805	480	11.83	3256	2272	3509

A. Crack patterns

Fig. 8a to 8h present the results of the crack development study on the tension surface of reinforced concrete slabs. Fig. 9a to 9h present the results of the crack view of the tension surface of all specimens after failure.

The control specimen, S1, showed the first cracks near the column at a load of approximately 24.4% of the experimental load capacity, developing radially from the edge of the column towards the supports. Further loading above 60% of the ultimate load resulted in the formation of cracks primarily in the column vicinity within a zone with a radius of 200 mm. By loading above 75% of the ultimate load resulted in the formation of cracks primarily in the column vicinity within a zone with a radius of 400 mm.

In comparison, the first cracks in the S2, S3 and S4 specimens formed mainly under the capitals at a load level of about 21%, 22%, and 23% of the experimental load capacity, with their value slightly larger than in the control slab. The cracks gradually extended towards the supports, and their course outside coincided with the mesh of main reinforcement. Increasing the load above 60-70% of the ultimate load resulted in the formation of cracks under the capitals within a zone with a radius of 300mm, 250 mm, and 200 mm for S2, S3 and S4 respectively.

The crack development study on the S5, S3, and S6 specimens showed that the first cracks mainly formed under the capitals at a load level of approximately 23.4%, 22%, and 21.6% of the experimental load capacity, respectively, with their value slightly larger than in the control slab. The cracks extended gradually towards the supports, following the course of the main reinforcement mesh. Further loading above 60-70% of the ultimate load resulted in the formation of cracks under the capitals within 200mm, 250mm, and 260 mm for S5, S3 and S6 respectively.

According to the crack development study on the S3, and S7 specimens, the first cracks primarily formed under the capitals at a load level of approximately 22%, and 20.2% of the experimental load capacity, respectively, with their value slightly larger than in the control slab. The cracks gradually extended towards the supports, following the path of the main reinforcement mesh. Further loading above 60-70% of the ultimate load resulted in the formation of cracks under the capitals within a range of 250mm, and 300mm for S3, and S7, respectively.

The crack development study conducted on the S3 and S8 specimens revealed that the initial cracks mostly formed under the capitals at a load level of approximately 22% and 18.5% of the experimental load capacity, respectively, with their value slightly larger than in the control slab. The cracks propagated gradually towards the supports, following the direction of the main reinforcement mesh. Further loading above 60-70% of the ultimate load resulted in the formation of cracks under the capitals within a range of 250mm and 500mm for S3 and S8, respectively.

Based on the crack development analysis of the S1, S3, S9 and S10 specimens, the initial cracks primarily occurred under the capitals at a load level of around 24.4%, 22%, 24.4 and 22.5% of the experimental load capacity, respectively. The cracks progressed gradually towards the supports, following the path of the main reinforcement mesh. As the load increased beyond 60-70% of the ultimate load, cracks emerged under the capitals within a range of 200mm, and 250mm for S1, and S3, respectively, but in S9 and S10 this crack is not completed as the eccentric load cause stress concentration in a one side.

The crack pattern on the tension surface of the slabs after failure revealed an intense concentration of cracks in the column vicinity within a range of about 900 mm for S1and S9, while all specimens had a larger range of intense cracking, defined by a radius of about 1100-1300 mm from the column edge. The study also showed that the hidden capital made of SHCC induced an effect similar to the application of shear reinforcement.
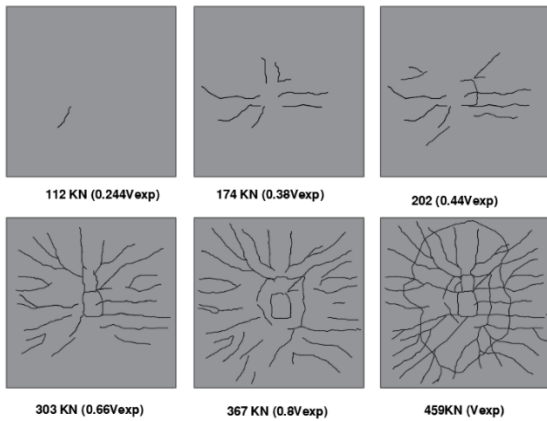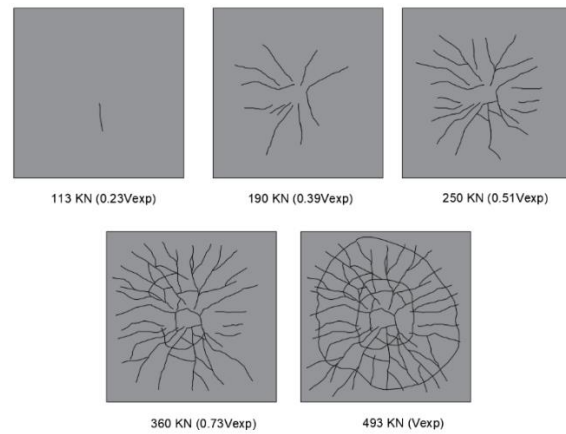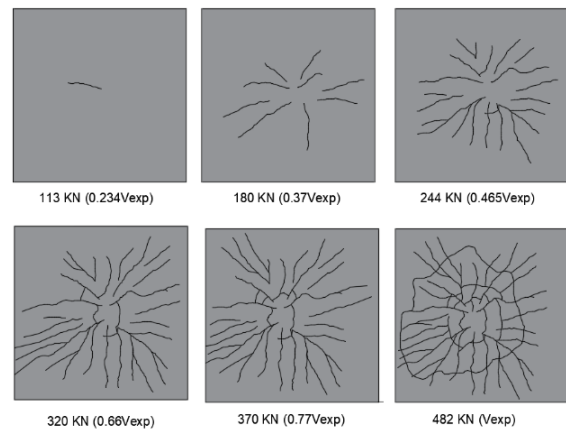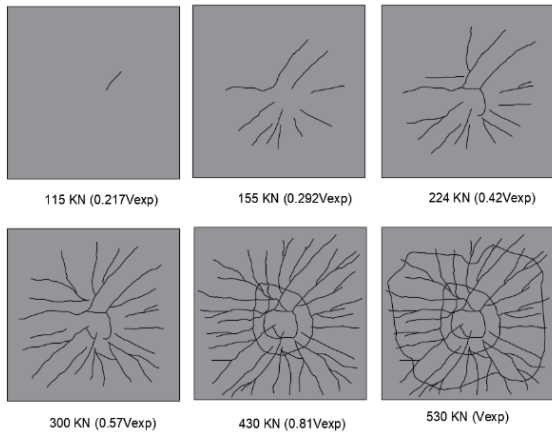

(a) Crack patterns of S1
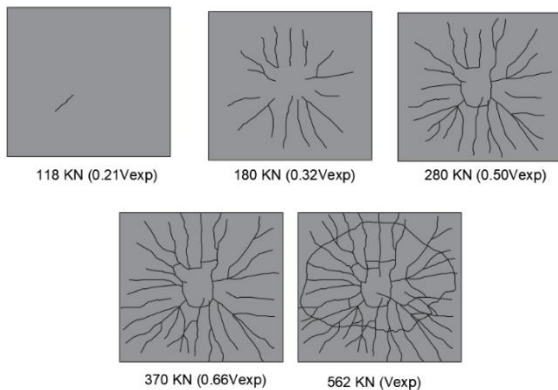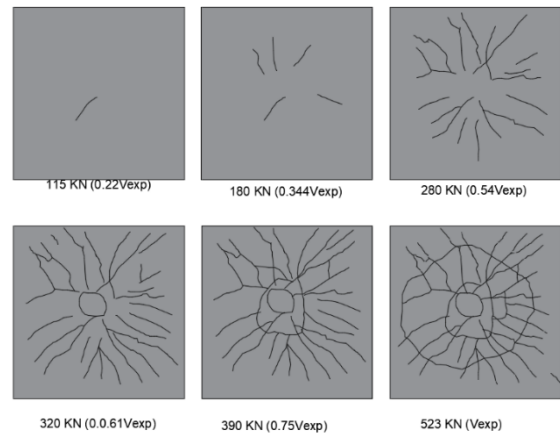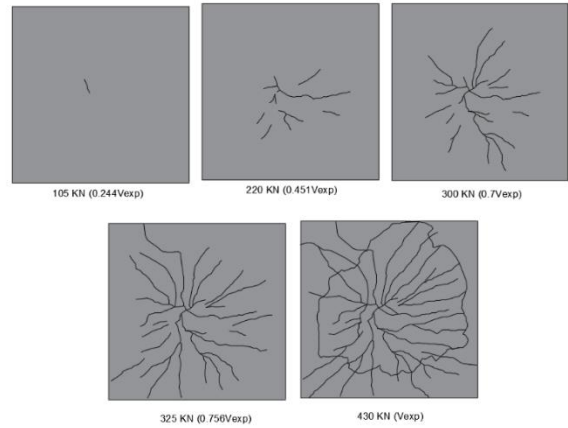

(b) Crack patterns of S2
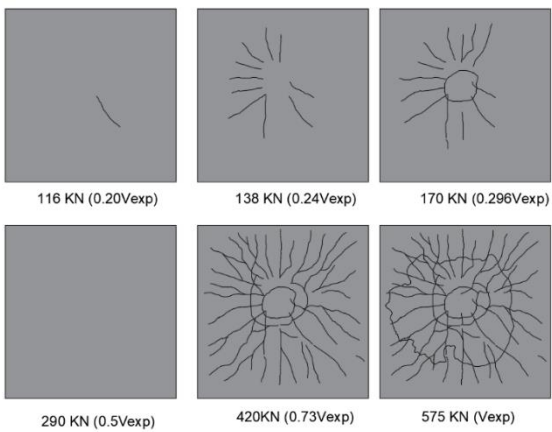

(c) Crack patterns of S3

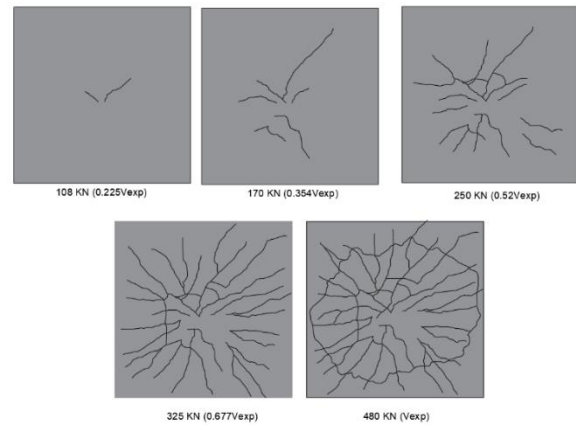

(d) Crack patterns of S4

(e) Crack patterns of S5

(f) Crack patterns of S6

(g) Crack patterns of S7
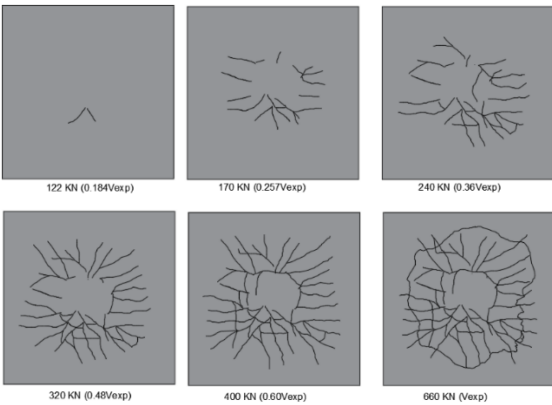

(h) Crack patterns of S8
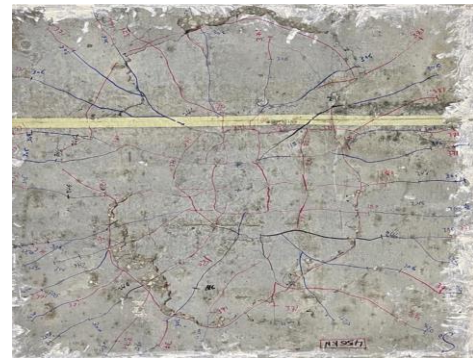

(i) Crack patterns of S9
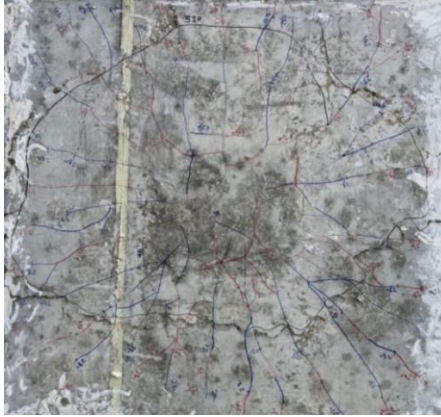

(j) Crack patterns of S10

Figure 8. Development of the crack pattern with respect to load level.

(a) Crack patterns of S1

(b) Crack patterns of S2

(c) Crack patterns of S3

(d) Crack patterns of S4

(e) Crack patterns of S5

(f) Crack patterns of S6

(g) Crack patterns of S7

(h) Crack patterns of S8

(i) Crack patterns of S9

(j) Crack patterns of S10

Figure 9. View of the tension surface of the specimens after failure.

B. *Mode of failure and shear crack*

Fig. 10a to 10h present the results of the crack patterns after failure of test slabs after saw-cut.

The load carrying capacity of the slabs was attained when a critical shear crack formed.

In the case of unstrengthen S1 and S9 specimens, the diagonal crack extended from the column edge towards the tension surface of the slab. Also, the shear cracks formed at the column edge and initially had an inclination angle of $\theta \approx 30 \div 40°$. One of the cracks changed its slope in the mid-height of the slab section, causing the course to become flatter.

In the slabs with a hidden capital, the critical shear cracks also formed at the column edge, but their initial inclination angle was smaller, approximately $20°$, allowing them to cross the capital at approximately half of its height. The course of the cracks in the part of the slab was similar, with an inclination angle of $\theta \approx 15°$, but after reaching the main reinforcement, they became clearly curved and flattened and its outlet was closer to the supports.

A significant change in the crack pattern was observed in the saw-cut of the S8 specimen. The thickness increased by the SHCC within the support zone was found to be highly effective. This resulted in an effect similar to increasing the slab thickness or column dimensions. The course of the cracks shown in Fig. 10h. In slab S8, it appears as though the crack has initiated after the face of the column by a distance that could be noticed if the SHCC portion was not taken into view. This resulted in an increase in the total width of the punching shear crack, which improved the performance of the specimen under loads.
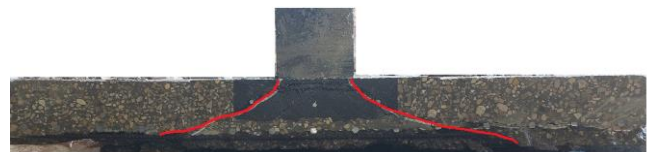

(a) Crack patterns of S1

(b) Crack patterns of S2

(c) Crack patterns of S3

(d) Crack patterns of S4

(e) Crack patterns of S5

90

(f) Crack patterns of S6

(g) Crack patterns of S7

(h) Crack patterns of S8

(i) Crack patterns of S9
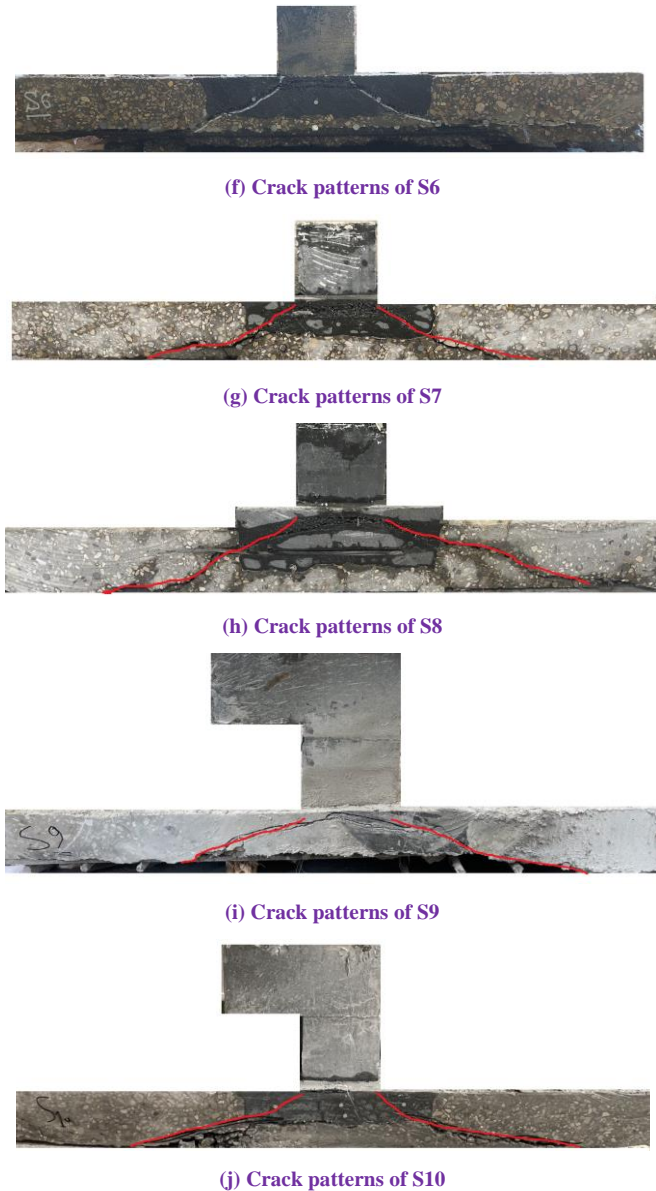

(j) Crack patterns of S10

Figure 10. Crack patterns of test slabs after saw-cut.

C. *Flexural cracking and ultimate loads*

Fig. 11 shows the effect of various parameters on cracking and ultimate loads.

From Fig. 11a, when comparing the flexural cracking load of slabs S4, S3, and S2 to the reference sample S1, it is evident that the flexural cracking load increased by 0.9%, 2.6%, and 5.5%, respectively, with an increase in the thickness of the SHCC layer by 0.25, 0.5, and 0.75 times the thickness of the flat slab in S4, S3 and S2 respectively. Furthermore, there was an increase in the ultimate load capacity by 7%, 14%, and 22% in samples S4, S3, and S2, respectively, as the thickness of the SHCC layer increased by 0.25, 0.5, and 0.75 times the thickness of the flat slab.
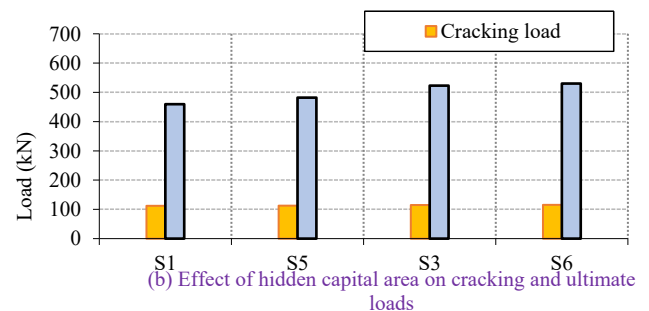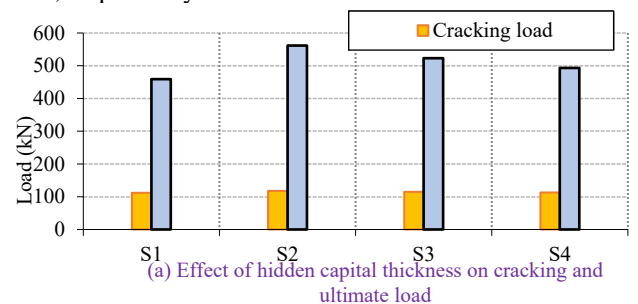
The results shown in Fig. 11b indicate that the flexural cracking load of S5, S3, and S6 increased by 0.5%, 2.6%, and 3.0%, respectively, when compared to the reference sample S1, as the extension of the SHCC layer increased by 0.5d, d, and 1.5d (d is the depth of the flat slab). Additionally,

there was an increase in the ultimate load capacity of S5, S3, and S6 by 5%, 14%, and 15%, respectively, with a corresponding increase in the extension of the SHCC layer by 0.5d, d, and 1.5d (d is the depth of the flat slab).

Based on the results presented in Fig. 11c, it can be observed that the flexural cracking load of S3, and S7 increased by 2.6%, and 3.7%, respectively, as the fiber content in the SHCC layer increased from 1% to 2% when compared to the reference slab S1. Furthermore, there was a corresponding increase in the ultimate load capacity of S3, and S7 by 14%, and 25.2%, respectively, as the fiber content in the SHCC layer increased from 1% to 2% when compared to the reference slab S1.

The results depicted in Fig. 11d demonstrate that an increase in the total depth of the SHCC layer outside the section by 0.0 and 0.25 slab thickness resulted in a 2.6% and 9.1% increase in the flexural cracking load of S3 and S8, respectively, when compared to the reference slab S1. Moreover, there was a corresponding increase in the ultimate load capacity of S3 and S8 by 14% and 34.8%, respectively, with an increase in the total depth of the SHCC layer outside the section by 0.0 and 0.25 slab thickness.

In terms of flexural cracking load and the effect of SHCC layer, S3, and S10 showed 2.6% higher values than the reference slabs S1 and S9, respectively. In terms of flexural cracking load and the effect of load eccentricity, S9, and S10 showed 6% to 6.6% lower values than the reference slabs S1 and S3, respectively. Regarding the impact of the SHCC layer on the ultimate load capacity, S3 and S10 exhibited a 11.6% to 14% increase in ultimate load compared to the reference slabs S1 and S9, respectively. However, when considering the effect of load eccentricity on the ultimate load, S9 and S10 showed a 6.4% to 8.22% decrease in ultimate load compared to the reference slabs S1 and S3, respectively.
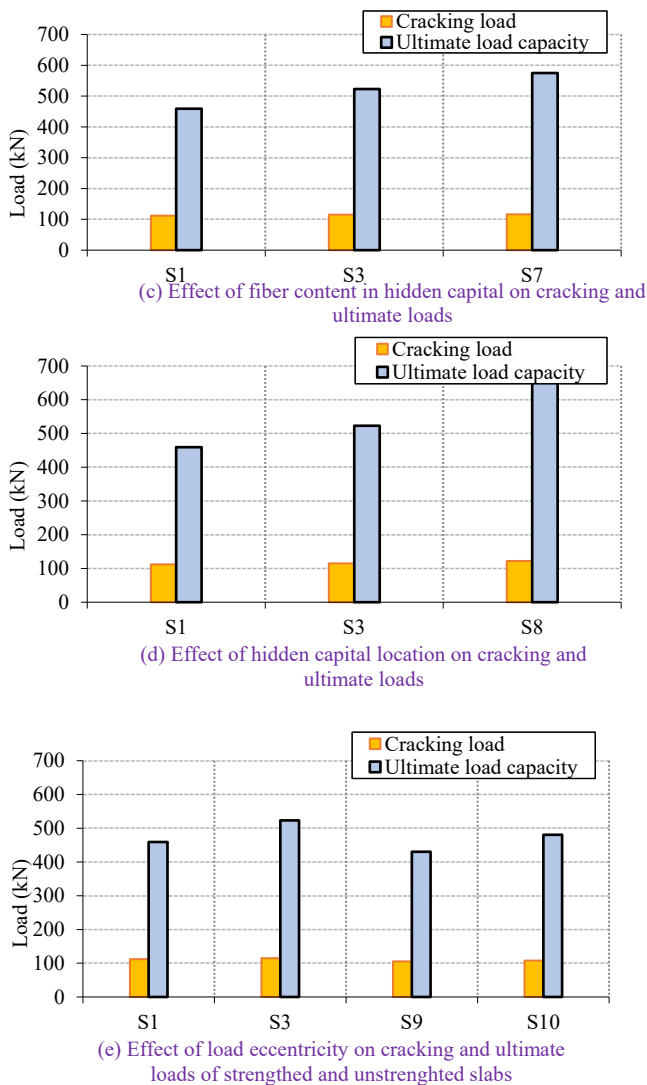

(a) Effect of hidden capital thickness on cracking and ultimate load

(b) Effect of hidden capital area on cracking and ultimate loads

91

(c) Effect of fiber content in hidden capital on cracking and ultimate loads

(d) Effect of hidden capital location on cracking and ultimate loads

(e) Effect of load eccentricity on cracking and ultimate loads of strengthed and unstrenghted slabs

Figure 11. Effect of various parameters on cracking and ultimate loads.

D. Deformations

From all the graphs in Figure 12, it is evident that the impact of all variables on the deflection values under loading is negligible, except for slabs S7 and S8. This is due to the increased of fiber content and thickness of the slab by placing a layer of SHCC with a thickness of 40 mm outside the section, resulting in an improvement in the deflection values under loading for the reference slab S1 by only 6%.

From Fig. 12a, when comparing the deflection at ultimate load of slabs S4, S3, and S2 to the reference slab S1, it is evident that the deflection at ultimate load increased by 5.7%, 9.6%, and 10%, respectively, with an increase in the thickness of the SHCC layer by 0.25, 0.5, and 0.75 times the thickness of the flat slab in S4, S3 and S2 respectively.
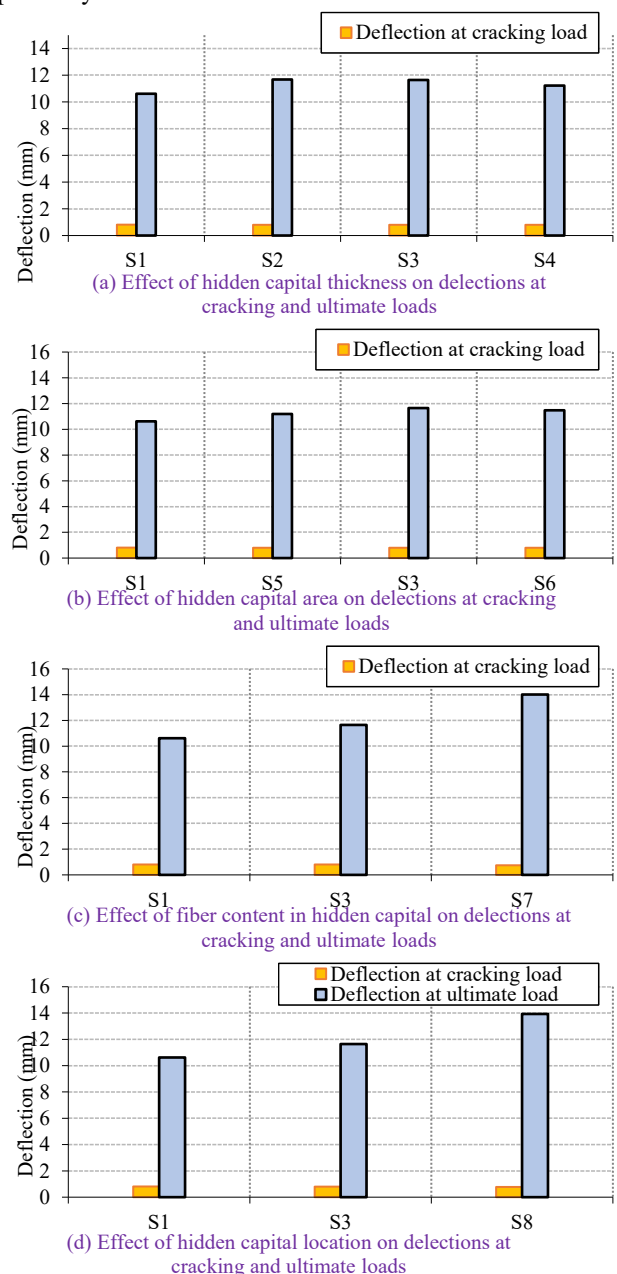
The results shown in Figure 12b indicate that the deflection at ultimate load of S5, S3, and S6 increased by 5.4%, 9.6%, and 8.0%, respectively, when compared to the reference sample S1, as the extension of the SHCC layer increased by 0.5d, d, and 1.5d (d is the depth of the flat slab).
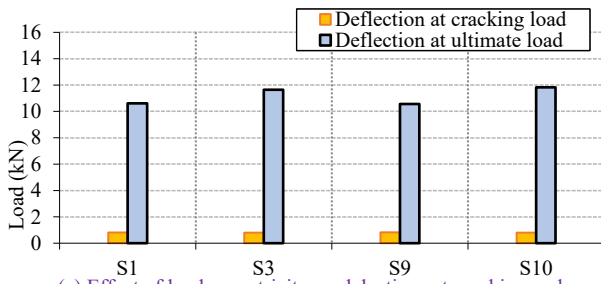
Based on the results presented in Figure 12c, it can be observed that the deflection at ultimate load of S3, and S7

increased by 9.6%, and 32.0%, respectively, as the fiber content in the SHCC layer increased from 1% to 2% when compared to the reference slab S1.

The results depicted in Fig. 12d demonstrate that an increase in the total depth of the SHCC layer outside the section by 0.0 and 0.25 slab thickness resulted in a 9.6% and 31.1% increase in the deflection at ultimate load of S3 and S8, respectively, when compared to the reference slab S1.

From the results depicted in Fig. 12e, regarding the impact of the SHCC layer on the deflection at ultimate load, S3 and S10 exhibited a 9.6% to 11.2% increase in ultimate load compared to the reference slabs S1 and S9, respectively. However, when considering the effect of load eccentricity on the ultimate load, S9 and S10 showed a 0.5% to 1.5% decrease in ultimate load compared to the reference slabs S1 and S3, respectively.

(a) Effect of hidden capital thickness on deflections at cracking and ultimate loads

(b) Effect of hidden capital area on deflections at cracking and ultimate loads

(c) Effect of fiber content in hidden capital on deflections at cracking and ultimate loads

(d) Effect of hidden capital location on deflections at cracking and ultimate loads

(e) Effect of load eccentricity on delections at cracking and ultimate loads of strengthed and unstrenghted slabs

Figure 12. Effect of various parameters on deflection at cracking and deflection at ultimate loads.

E. Load deflection response

This part describes the results of a study that investigated the effect of different variables of a practical program on the load-deflection curve for all tested specimens. Fig. 13 shows the load-deflection curve which is a graphical representation of the relationship between the applied load and the resulting deformation of a test slabs.

The curves consist of three parts, and the first part is linear and represents the loading from the beginning until the first crack occurs. The initial stiffness of the test slabs converges significantly, except for S8, which showed a slightly different stiffness. The second part of the curve is located between the beginning of the cracking point and the maximum load. Differences were observed between all slabs, where the slabs strengthed with a SHCC layer of mortar showed a clear improvement in the bending stiffness. The bending stiffness increased with the increase in thickness of the SHCC layer, the increase in the area of the SHCC layer, the increase in the fiber content in the SHCC layer, and the increase in the thickness of the SHCC layer outside the concrete slab. The bending stiffness reflects the resistance of the slabs to deformation, and all of this is attributed to the elastic modulus of the concrete and the SHCC layer used in the strength operation.

The third part of the curve begins from the maximum load point until the end of the loading phase and represents the post-peak phase. In general, all slabs show the same slope of the load-deflection curve after the maximum limit. Additionally, the strengthed slabs generally maintain a higher load value after collapse, which makes the strength layer an ideal layer for post-collapse to reduce total collapses.

Overall, the study of load deflection curves shows the importance of SHCC layers in improving the bending stiffness and improve the slabs resistance to deformation. The findings can be used to optimize the design and material selection for various applications, including those that require high strength and durability.

From Fig. 13, by comparing the deflection at 0.93% of the ultimate load of slab S1 (at 427.7 kN) for all slabs, the benefits of the reinforcement layer in restricting deformation become apparent. By comparing S4, S3, and S2 to the reference slab S1, it is evident that the deflection decreased by 8%, 9%, and 16%, respectively, with an increase in the thickness of the SHCC layer by 0.25, 0.5, and 0.75 times the thickness of the flat slab in S4, S3, and S2, respectively, Fig. 13a. For S5, S3,

and S6 the deflection decreased by 4.5%, 9%, and 9.2%, respectively, when compared to the reference slab S1, as the extension of the SHCC layer increased by 0.5d, d, and 1.5d (d is the depth of the flat slab), Fig. 13b. For S3 and S7 the deflection decreased by 9% and 11%, respectively, as the fiber content in the SHCC layer increased from 1% to 2% when compared to the reference slab S1, Fig. 13c. The results depicted in Fig. 13d demonstrate that an increase in the total depth of the SHCC layer outside the section by 0.0 and 0.25 slab thickness resulted in a 9% and 22% decrease in the deflection for S3 and S8, respectively, when compared to the reference slab S1, Fig. 13d. From the results depicted in Fig. 14e, regarding the impact of the SHCC layer on the deflection, S3 and S10 exhibited a 9% to 5.5% decrease in deflection compared to the reference slabs S1 and S9, respectively. However, when considering the effect of load eccentricity on the tension strain, S9 and S10 showed a 8% to 12.3% increase in tension strain compared to the reference slabs S1 and S3, respectively.
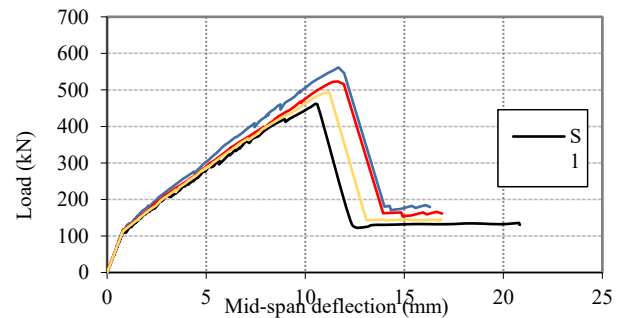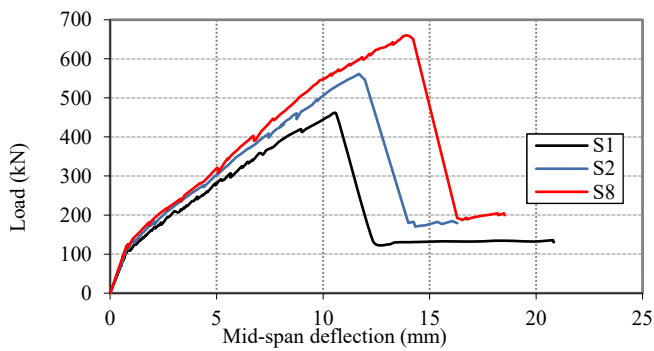

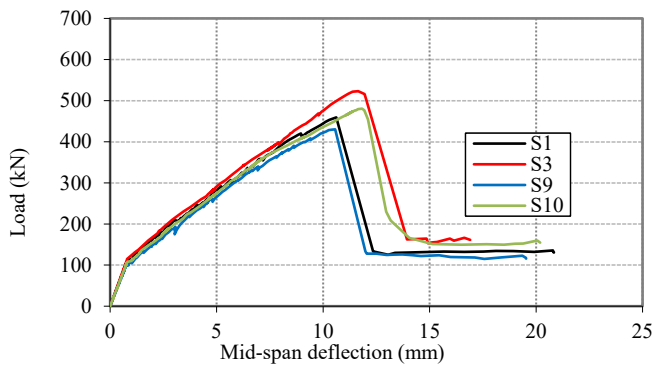**(a) Effect of hidden capital thickness on load-mid span deflection**
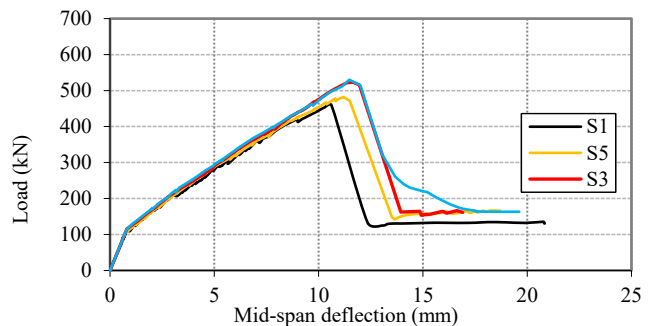
(b) Effect of hidden capital area on load-mid span deflection
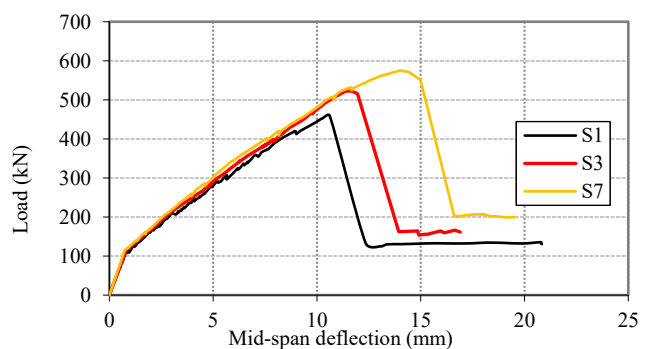
(c) Effect of fiber content in hidden capital on load-mid span deflection

(d) Effect of hidden capital location on load-mid span deflection

(e) Effect of load eccentricity on load-mid span deflection of strengthed and unstrenghted slabs

Figure 13. Effect of various parameters on load-mid span deflection.

F. Strains

Compression concrete strains: The comparison of strains measured on the compressed side of the slabs is presented in Fig. 14. A significant difference in the intensity of deformations can be observed between the control slab S1 and the specimens with hidden capitals. This difference can be attributed to the higher strength of SHCC, which has a modulus of elasticity that is about 44% higher than plain concrete. Compression strains at d/2 from column face varied from 0.9 to 0.75 for all slabs except S8 with hidden capital compared with reference slabs S1 and S9, respectively. This indicates that stresses measured on the capital's surface were around 10% to 25% lower. The stresses increased immediately before failure of all specimens, which accounted for about 40% of the ultimate strains. In slab S8, at approximately 90% of the load carrying capacity of the control specimen, a decrease in the concrete deformation by up to 46% was observed. This can be attributed to the increased depth of the sector in this area, as well as the high resistance of the reinforcement layer, which also gives a significant difference in the modulus of elasticity.

From Fig. 14a, when comparing the compression strain at 0.93% of the ultimate load of slab S1 (at 430 kN) for slabs S4, S3, and S2 to the reference slab S1, it is evident that the concrete compression strain decreased by 11.7%, 14.3%, and 17.6%, respectively, with an increase in the thickness of the SHCC layer by 0.25, 0.5, and 0.75 times the thickness of the flat slab in S4, S3 and S2 respectively.

The results shown in Fig. 14b indicate that the compression strain at 0.93% of the ultimate load of slab S1 (at 430 kN) for S5, S3, and S6 decreased by 10%, 14.3%, and 22.8%, respectively, when compared to the reference slab S1, as the extension of the SHCC layer increased by 0.5d, d, and 1.5d (d is the depth of the flat slab).

Based on the results presented in Fig. 14c, it can be observed that the compression strain at 0.93% of the ultimate load of slab S1 (at 430 kN) for S3, and S7 increased by 14.3%, and 28.1%, respectively, as the fiber content in the SHCC layer increased from 1% to 2% when compared to the reference slab S1.

The results depicted in Fig. 14d demonstrate that an increase in the total depth of the SHCC layer outside the section by 0.0 and 0.25 slab thickness resulted in a 14.3% and 44.8% decrease in the compression strain at 0.93% of the ultimate load of slab S1 (at 430 kN) for S3 and S8, respectively, when compared to the reference slab S1.

From the results depicted in Fig. 14e, regarding the impact of the SHCC layer on the compression strain at 0.93% of the ultimate load of slab S1 (at 430 kN), S3 and S10 exhibited a 15.3% to 10.7% increase in compression strain compared to the reference slabs S1 and S9, respectively. However, when considering the effect of load eccentricity on the the compression strain at 0.93% of the ultimate load of slab S1 (at 430 kN) load, S9 and S10 showed a 13.5% to 21.0% increase in compression strain compared to the reference slabs S1 and S3, respectively.

Tension steel strains: Fig. 14 shows the impact of different variables of the practical program on the load-tension strain curves for all tested specimens, with a particular focus on the effect of reinforcement on the tensile side of the curve. The curves are divided into two parts, with the first part representing the linear loading from the beginning until the first crack occurs. In this part, all slabs were almost identical, except for sample number 8, which showed a slightly different linear part. the reasons explained in the previous load and deformation sections.

The second part of the load-deflection curve is between the beginning of the cracking point and the maximum load, where differences were observed between slabs. slabs reinforced with a layer of mortar showed a clear improvement in the steel strains on the tensile side of the curves. The strains in steel decreased with the increase in thickness of the SHCC layer, the increase in the area of the SHCC layer, the increase in the fiber content in the SHCC, and the increase in the thickness of the SHCC layer outside the concrete section. The load-strain curves of strengthed slabs reflect the resistance of the slabs to deformation, and all of this is attributed to the elastic modulus of the concrete and the mortar used in the strength.

From Fig. 14a, when comparing the tension strain at 0.93% of the ultimate load of slab S1 (at 430 kN) for slabs S4, S3, and S2 to the reference slab S1, it is evident that the tension strain decreased by 12.2%, 11.1%, and 5.2%, respectively, with an increase in the thickness of the SHCC layer by 0.25, 0.5, and 0.75 times the thickness of the flat slab in S4, S3, and S2, respectively.
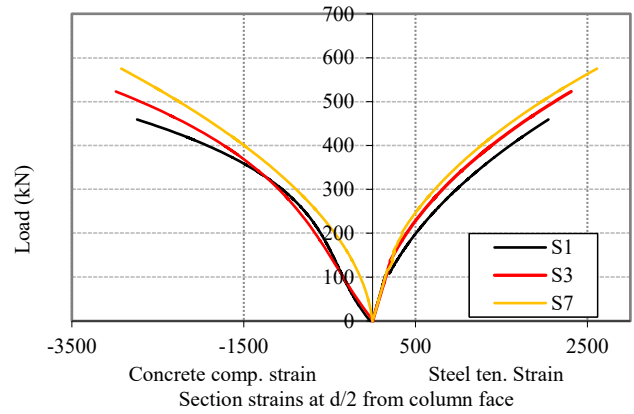
94

The results shown in Fig. 14b indicate that the tension strain at 0.93% of the ultimate load of slab S1 (at 430 kN) for S5, S3, and S6 increased by 0.9%, 11.1%, and 16.0%, respectively, when compared to the reference slab S1, as the extension of the SHCC layer increased by 0.5d, d, and 1.5d (d is the depth of the flat slab).

Based on the results presented in Fig. 14c, it can be observed that the tension strain at 0.93% of the ultimate load of slab S1 (at 430 kN) for S3 and S7 decreased by 11.1% and 17.9%, respectively, as the fiber content in the SHCC layer increased from 1% to 2% when compared to the reference slab S1.

The results depicted in Fig. 14d demonstrate that an increase in the total depth of the SHCC layer outside the section by 0.0 and 0.25 slab thickness resulted in a 11.1% and 38.6% decrease in the tension strain at 0.93% of the ultimate load of slab S1 (at 430 kN) for S3 and S8, respectively, when compared to the reference slab S1.
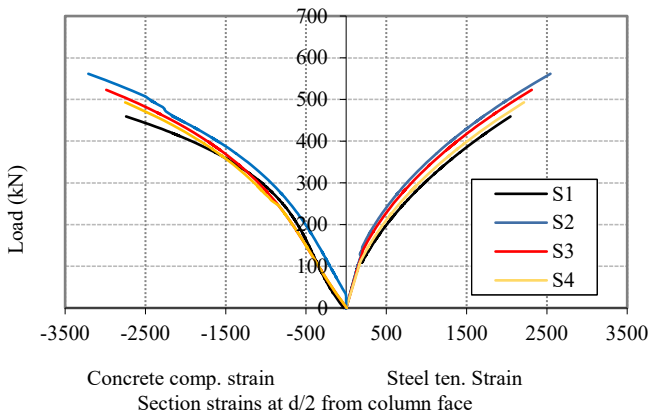
From the results depicted in Fig. 14e, regarding the impact of the SHCC layer on the tension strain at 0.93% of the ultimate load of slab S1 (at 430 kN), S3 and S10 exhibited a 10% to 4.7% decrease in tension strain compared to the reference slabs S1 and S9, respectively. However, when considering the effect of load eccentricity on the tension strain at 0.93% of the ultimate load of slab S1 (at 430 kN), S9 and S10 showed a 10.7% to 11.9% increase in tension strain compared to the reference slabs S1 and S3, respectively.

(a) Effect of hidden capital thickness on concrete and steel strains

(b) Effect of hidden capital area on concrete and steel strains

(c) Effect of fiber content in hidden capital on concrete and steel strains
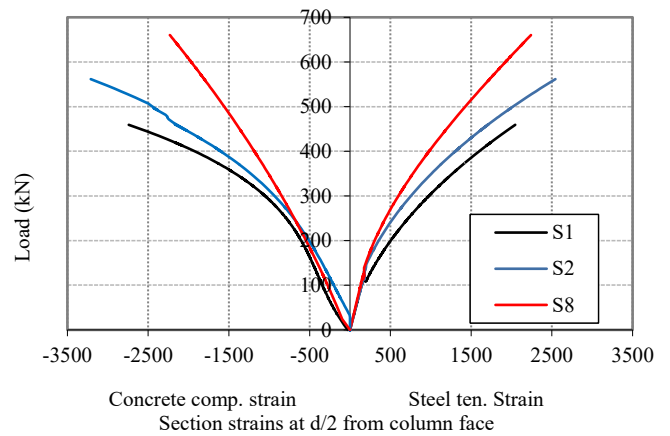
(d) Effect of hidden capital location on concrete and steel strains
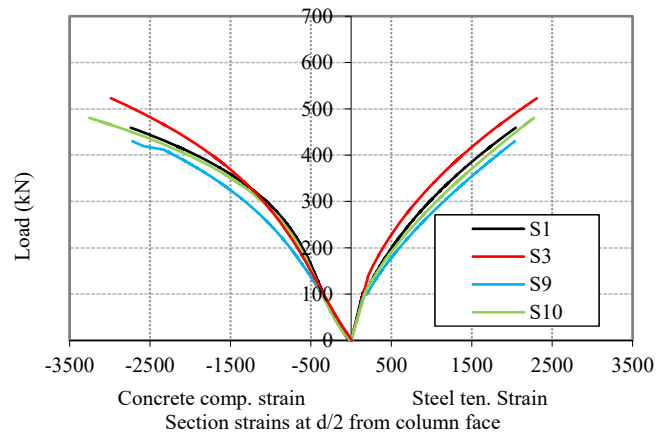
(e) Effect of load eccentricity on concrete and steel strains of strengthed and unstrenghted slabs

Figure 14. Effect of various parameters on concrete compression strain and steel tension strains for all slabs.

G. Ductility

Previous research has used a variety of indicators to assess ductility, with energy absorption being one of the most important indicators. The area under the load-deflection curves up to the maximum load, indicated as E, represents

energy absorption. As predicted, the control Slab S1 had the lowest energy absorption value and S8 had the largest value. Fig. 15 compares the energy absorption results for every parameter.

From Fig. 15a, when comparing ductility for slabs S4, S3, and S2 to the reference slab S1, it is evident that ductility increased by 12.6%, 22.4%, and 30.1%, respectively, with an increase in the thickness of the SHCC layer by 0.25, 0.5, and 0.75 times the thickness of the flat slab in S4, S3, and S2, respectively. The results shown in Fig. 14b indicate that the ductility for S5, S3, and S6 increased by 10.8%, 22.4%, and 23.2%, respectively, when compared to the reference slab S1, as the extension of the SHCC layer increased by 0.5d, d, and 1.5d (d is the depth of the flat slab). Based on the results presented in Fig. 14c, it can be observed that the ductility for S3 and S7 increased by 22.4% and 69.5%, respectively, as the fiber content in the SHCC layer increased from 1% to 2% when compared to the reference slab S1. The results depicted in Fig. 14d demonstrate that an increase in the total depth of the SHCC layer outside the section by 0.0 and 0.25 slab thickness resulted in a 22.4% and 85.4% increase in the ductility for S3 and S8, respectively, when compared to the reference slab S1. From the results depicted in Fig. 14e, regarding the impact of the SHCC layer on the ductility, S3 and S10 exhibited a 22.4% to 24.6% increase in ductility compared to the reference slabs S1 and S9, respectively. However, when considering the effect of load eccentricity on the ductility, S9 and S10 showed a 5.8% to 4.1% decrease in ductility compared to the reference slabs S1 and S3, respectively.

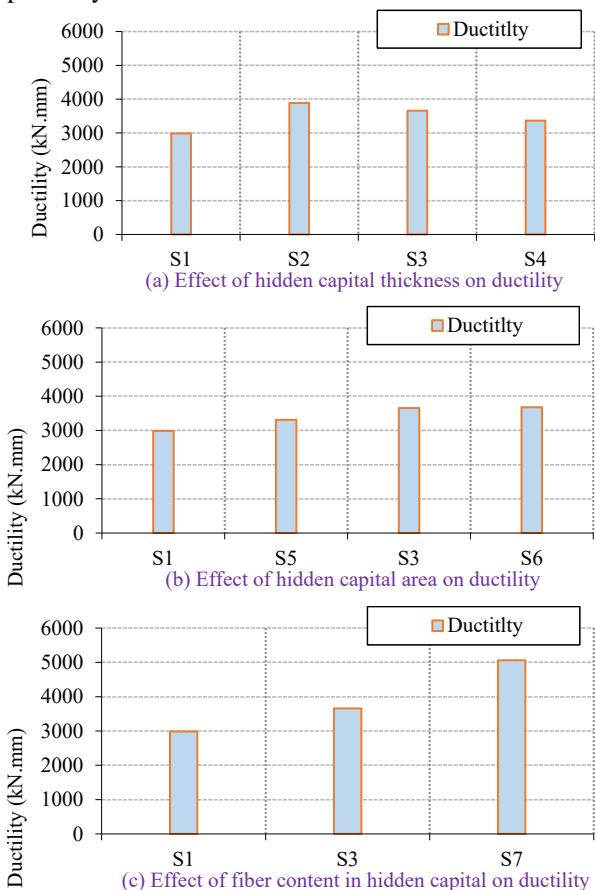(a) Effect of hidden capital thickness on ductility

(b) Effect of hidden capital area on ductility

(c) Effect of fiber content in hidden capital on ductility

(d) Effect of hidden capital location on ductility

(e) Effect of hidden capital location on ductility

Figure 15. Effect of various parameters on ductility of slabs.

V-   CALCULATION OF ULTIMATE CAPACITY OF SLAB-COLUMN CONNECTIONS

A concrete slab's punching shear strength is calculated by computing a nominal shear stress on a critical shear perimeter which located at a distance from the column faces. Different codes of practise prescribe different punching shear formula and different critical shear boundary position. One code may differ significantly from another.

A.   ACI 318-19 method [28]:

based on the concrete cylinder's compressive strength(f'_c), the punching shear strength of slabs without shear reinforcement may be calculated using the lowest of the following formulas according to ACI 318-19 [28].

$$V_c = 0.33\lambda_s\sqrt{f'_c}.b_o.d \qquad (1)$$

$$V_c = 0.083\left(\frac{\alpha_s d}{b_o} + 2\right)\lambda_s\sqrt{f'_c}.b_o.d \qquad (2)$$

$$V_c = 0.17\left(\frac{2}{\beta} + 1\right)\lambda_s\sqrt{f'_c}.b_o.d \qquad (3)$$

Where $\lambda_s = \sqrt{\frac{2}{1+0.004d}} \leq 1.0$, β is the ratio of the longer

side to the shorter side of the concentrated load (or column) f'_c is the cylinder concrete strength is assumed as 0.8 f_{cu}, α_s is 40 for interior columns, 30 for edge columns, and 20 for edge columns. The value b_o is the length of critical shear perimeter taken at a distance of 0.5d away from the column face and has square corners for square columns and rounded corners for circular columns.

The ACI 318-19 [28] approach clearly overlooks the role of flexural reinforcement on punching shear capacity. Table 6 shows a comparison between experimental slab capacities and ACI 318-19 [28] .

B. Euro code 2 (2020) [27]:

According to Euro code 2 (2020) [27], the punching shear strength of slabs without shear reinforcement is given by:

$$V_c = 0.6 k_{pb}(100\rho f_{ck}\frac{d_{dg}}{a_p})^{\frac{1}{3}}.b_o.d \leq 0.6\sqrt{f_{ck}} \quad (4)$$

$$k = 3.6\left(1 + \frac{b_o}{d_{0.5}}\right)^{0.5} < 2.5 \quad and\ a_p = \left(\frac{a_{p.dv}}{8}\right)^{0.5} \quad (5)$$

The formula involves the following variables: k_{pb}: shear gradient enhancement factor, d_v: shear effective depth, b_0: length of the column periphery, a_p: distance from the centre of the control perimeter to the point where bending moments are zero, ρ_l: flexural reinforcement ratio, f_{ck}: characteristic value of the concrete compressive strength, d_{dg}: factor taking into account the influence of the maximum aggregate size, 16mm + D_{lower}<40 for normal strength concrete, D_{lower} : smallest value of the upper sieve size D in an aggregate for the coarsest fraction of aggregates in the concrete permitted by the specification of concrete. The critical shear parameter is located from $0.50d_v$ up to a distance of $0.67d_v$ from the face of the column.

Table 6 compares experimental slab capacities to Euro code2 (2020) [27].

C. ECP 203-2018 [25]:

According to ECP 203-2018, the punching shear strength of slabs can be determined from the lowest of the following expressions (in N, mm units)

$$Q_{up} = 0.8[\ (\alpha\ d/b_o)+0.2]\ \sqrt{f_{cu}}\ .b_o.d \quad (7)$$

$$Q_{up} = 0.316[\ (a/b)+0.5]\ \sqrt{f_{cu}}\ .b_o.d \quad (8)$$

$$Q_{up} = 0.316\sqrt{f_{cu}}\ .b_o.d \quad (9)$$

where a and b are the shorter and the longer side of the concentrated load (or column)

α is 4.0 for interior columns, 3.0 for edge columns, and 2.0 for edge columns.

The value b_o is the length of critical shear perimeter taken at a distance of 0.5d away from the column face and has square corners for square columns and rounded corners for circular columns.

The ECP 203-2018 [25] approach clearly overlooks the role of flexural reinforcement and size effect on punching shear capacity. Table 6 shows a comparison of experimental slab capacities to ECP 203-2007.

D. Proposed equation:

prediction of the flat slab punching shear is the aim of the different research. The main advantages of T.F El-Shafeiy al [5]. equation is simplicity for using by engineers and it is accurate more than other code methods. Because of these reasons we will modify the same equation to give more precise prediction of the ultimate punching shear. The equation introduced a coefficient C obtained by regression analysis of the experimental results and numerical analysis.

$$V_c = C\ (\rho)^{1/3}\ (f_c')^{1/3}\ .b_o.d \quad \text{in MPa} \quad (10)$$

Where The coefficient C = 0.8   for solid slabs

E. Results

From the results of table 6, it is clear that the least conservative equation is the Egyptian code ECP 203-2018 [25] , followed by the American code ACI 318-19 [28], and finally the most conservative equation is the European code Euro code 2 (2020) [27]. Therefore, it is recommended to use the Egyptian code equation with dividing the depth of the strengthening layer having similar calculations as for the concrete layer, and each having its own thickness.

Table 6. Codes models and proposed model results.

Slab	Ultimate experimental load (kN)	ACI 318-19 (kN)	Euro code 2 (2020) (kN)	ECP 203-2007 (kN)	Proposed equation (kN)
S1	459.2	279.3	251.3	299.0	409.4
S2	561.5	389.4	350.5	416.9	510.5
S3	523	352.7	317.4	377.6	476.8
S4	492.9	316.0	284.4	338.3	443.1
S5	482.1	352.7	317.4	377.6	476.8
S6	530	352.7	317.4	377.6	476.8
S7	575.1	372.3	335.1	398.6	493.6
S8	660.2	539.8	485.8	609.4	756.2

VI- CONCLUSION

The use of SHCC hidden capitals in slab-column connections can have a positive impact on their cracking behavior and failure mode. The thickness, area, and fiber content ratio of the SHCC layer have a negligible effect on increasing the cracking load and decreasing deflection at cracking. However, increasing the partition of SHCC outside the slab can significantly increase the cracking load and decrease deflection. Furthermore, the thickness and fiber content of the SHCC layer have a significant impact on the ultimate punching capacity, flexural cracking load, deflection, concrete compression strain, tension strain, and ductility. Finally, strengthening these slabs can significantly improve their punching capacity. Based on the results of the experimental program, these recommendations can be formulated:

1. The use of SHCC hidden capitals can effectively improve the cracking behavior and mode of failure. Due to the decrease in the severity of the crack inclination, the formation of cracks at the tension side occurred within a larger radius than in the control specimens.

2. The hidden capital's thickness, area, and fiber content ratio in the SHCC have a negligible effect to increase the cracking load by a range between 0.9% to 5.5% and decreasing deflection at cracking by a range between 0.75% to 1.4%. However, increasing the partition of SHCC outside the slab by 0.25 of the slab thickness increases the cracking load by 9.5% and decreases the deflection by 4.5%.

3. The ultimate punching capacity increased by 7%, 14%, and 22%, the flexural cracking load increased by 0.9%, 2.6%, and 5.5%, the deflection decreased by 8%, 9%, and 16%, the concrete compression strain decreased by 17.6%, 14.3%, and 11.7%, the tension strain decreased by 12.2%, 11.1%, and 5.2%, and the ductility increased by 12.6%, 22.4%, and 30.1%,   as the thickness of the SHCC layer increased by 0.25, 0.5, and 0.75 times the slab thickness respectively.

4. The ultimate punching capacity increased by 5%, 14%, and 15%, the flexural cracking load increased by 0.5%, 2.6%, and 3.0%, the deflection decreased by 4.5%, 9%, and 9.2%, the compression strain decreased by 10%, 14.3%, and 22.8%, the tension strain decreased by 0.9%, 11.1%, and 16.0%, and the ductility increased by 10.8%, 22.4%, and 23.2%, with a corresponding increase in the extension of the SHCC layer by 0.5, 1.0, and 1.5 the slab depth respectively.

5. The ultimate punching capacity increase by 14%, and 25.2%, the flexural cracking load increased by 2.6%, and 3.7%, the deflection decreased by 9% and 11%, and 8.0%, the compression strain decreased by 14.3%, and 28.1% the tension strain decreased by 11.1% and 17.9%, and the ductility increased by 22.4% and 69.5% as the fiber content in the SHCC layer increased from 1% to 2% respectively.

6. Corresponding increase in the ultimate punching capacity by 14% and 34.8%, increase in the flexural cracking load by 2.6% and 9.1% decrease in the deflection by 9% and 22%, decrease in the compression strain by 14.3% and 44.8%, and decrease in the tension strain by 11.1% and 38.6%, and increase in the ductility by 22.4% and 85.4%, with an increase in the total depth of the SHCC layer outside the section by 0.0 and 0.25 slab thickness respectively.

7. In the case of shifting the test load by 100 mm, the cracking load decreased by average 6.3%. While the ultimate punching capacity decreased by average 6.5% and negligible effect was notice in deflections. Strengthening these slabs increase the punching capacity by average 12.7%.

8. Comparison with various world codes showed that the Egyptian code calculations involve a high degree of accuracy and are closest to the results of laboratory tests.

9. The least conservative equation is the Egyptian code ECP 203-2018 [25] , followed by the American code ACI 318-19 [28], and finally the most conservative equation is the Euro code 2 (2020) [27].

REFERENCES

[1] "Acknowledgement to Reviewers of Buildings in 2016," Buildings, vol. 7, no. 4, p. 7, Jan. 2017, doi: 10.3390/buildings7010007.

[2] H. S. Shukla and M. Tamsir, "Extended modified cubic B-spline algorithm for nonlinear Fisher's reaction-diffusion equation," Alexandria Eng. J., vol. 55, no. 3, pp. 2871–2879, Sep. 2016, doi: 10.1016/j.aej.2016.06.031.

[3] P. Deivajothi, V. Manieniyan, and S. Sivaprakasam, "An impact of ethyl esters of groundnut acid oil (vegetable oil refinery waste) used as emerging fuel in DI diesel engine," Alexandria Eng. J., vol. 57, no. 4, pp. 2215–2223, Dec. 2018, doi: 10.1016/j.aej.2017.09.003.

[4] E. Tosun and A. Çalık, "Failure load prediction of single lap adhesive joints using artificial neural networks," Alexandria Eng. J., vol. 55, no. 2, pp. 1341–1346, Jun. 2016, doi: 10.1016/j.aej.2016.04.029.

[5] "TF EL-Shafiey, M Hussein, & MA Abdel-Aziz,(2012)' BEHAVIOUR OF FLAT SLABS WITH OPENINGS ADJACENT TO COLUMNS,' STRUCTURAL FAULTS & REPAIR-2012 14th International Conference 3rd-5th July 2012 Edinburgh, Scotland, Concrete Behaviour Part (CB), CB-AZIZ code."

[6] C. C. Thong, D. C. L. Teo, and C. K. Ng, "Application of polyvinyl alcohol (PVA) in cement-based composite materials: A review of its engineering properties and microstructure behavior," Constr. Build. Mater., vol. 107, pp. 172–180, Mar. 2016, doi: 10.1016/j.conbuildmat.2015.12.188.

[7] "Fakharifar, M., & Ettefagh, M. M. (2017). Experimental study on the effect of fiber-reinforced polymer (FRP) strengthening on the punching shear strength of flat slab-column connections. Journal of Rehabilitation in Civil Engineering, 5(4), 1-11. doi: 10.," doi: 10.22075/jrce.2017.11276.1198.

[8] "Cheung, M. S., & Kuchma, D. A. (2002). Punching shear strength of flat reinforced concrete slabs. ACI Structural Journal, 99(6), 772-780."

[9] N. Hooda, "Analysis of Flat Slab Connection System for Seismic Loads," Engineering, 2018.

[10] S. M. and A. Ghali, "Cautionary Note on Shear Capitals," Concr. Int., vol. 24, no. 3, pp. 75–82, 2002.

[11] R. Pang, L. Dang, H. Ni, S. Liang, and Q. Li, "Experimental study on punching shear behavior of hollow floor slab-column reinforced connection," Adv. Struct. Eng., vol. 22, no. 7, pp. 1531–1543, May 2019, doi: 10.1177/1369433218819565.

[12] M. Gołdyn and T. Urban, "Hidden Capital as an Alternative Method for Increasing Punching Shear Resistance of LWAC Flat Slabs," Arch. Civ. Eng., vol. 65, no. 4, pp. 309–328, Dec. 2019, doi: 10.2478/ace-2019-0062.

[13] M. Gołdyn and T. Urban, "UHPFRC hidden capitals as an alternative method for increasing punching shear resistance of LWAC flat slabs," Eng. Struct., vol. 271, no. August, 2022, doi: 10.1016/j.engstruct.2022.114906.

[14] J. Bartol, "Problem of punching shear in slabs on culumns," Engineering, 2007, [Online]. Available: https://www.semanticscholar.org/paper/Problem-of-punching-shear-in-slabs-on-culumns-Bartol/1b8208f7adef72b4898210c37db44d8312442a07.

[15] K. Yu, L. Li, J. Yu, Y. Wang, J. Ye, and Q. Xu, "Direct tensile properties of engineered cementitious composites: A review," Constr. Build. Mater., vol. 165, pp. 346–362, Mar. 2018, doi: 10.1016/j.conbuildmat.2017.12.124.

[16] M. Kunieda, M. Hussein, N. Ueda, and H. Nakamura, "Enhancement of Crack Distribution of UHP-SHCC under Axial Tension Using Steel Reinforcement," J. Adv. Concr. Technol., vol. 8, no. 1, pp. 49–57, Feb. 2010, doi: 10.3151/jact.8.49.

[17] L.-Z. Li, Y. Bai, K.-Q. Yu, J.-T. Yu, and Z.-D. Lu, "Reinforced high-strength engineered cementitious composite (ECC) columns under eccentric compression: Experiment and theoretical model," Eng. Struct., vol. 198, p. 109541, Nov. 2019, doi: 10.1016/j.engstruct.2019.109541.

[18] L. Li, Z. Cai, K. Yu, Y. X. Zhang, and Y. Ding, "Performance-based design of all-grade strain hardening cementitious composites with compressive strengths from 40 MPa to 120 MPa," Cem. Concr. Compos., vol. 97, pp. 202–217, Mar. 2019, doi: 10.1016/j.cemconcomp.2019.01.001.

[19] Y. M. Lim and V. C. Li, "Durable repair of aged infrastructures using trapping mechanism of engineered cementitious composites," Cem. Concr. Compos., vol. 19, no. 4, pp. 373–385, Jan. 1997, doi: 10.1016/S0958-9465(97)00026-7.

[20] P. SUTHIWARAPIRAK, T. MATSUMOTO, and T. KANDA, "FLEXURAL FATIGUE FAILURE CHARACTERISTICS OF AN ENGINEERED CEMENTITIOUS COMPOSITE AND POLYMER CEMENT MORTARS," Doboku Gakkai Ronbunshu, vol. 2002, no. 718, pp. 121–134, Nov. 2002, doi: 10.2208/jscej.2002.718_121.

[21] "Till, R. Final Report on Durable Link Slabs for Jointless Bridge Decks Based on Strain-Hardening Cementitious Composites By M . Lepech , S . Qian , M . Weimann and S . Wang The Advanced Civil Engineering Material Research Laboratory Department of Civil an."

[22] H. M. Afefy, M. A. Abdel-Aziz, N. M. Kassem, and M. H. Mahmoud, "Improving flexural performance of post-tensioned pre-cast pre-stressed RC segmental T-beams," Structures, vol. 24,

pp. 304–316, Apr. 2020, doi: 10.1016/j.istruc.2020.01.027.

[23] mahmoud Abdelaziz, E. Etman, M. Hussien, and N. Kasem, "Enhancing the behavior of R.C. Continuous-Defected Slabs Using Strain-Hardening Cementitious Composites (SHCC)," J. Eng. Res., vol. 7, no. 2, pp. 0–0, May 2023, doi: 10.21608/erjeng.2023.212986.1182.

[24] G. Elsamak, A. Abdullah, M. I. Salama, J. W. Hu, and M. A. El-Mandouh, "Punching Shear Behavior of Slabs Made from Different Types of Concrete Internally Reinforced with SHCC-Filled Steel Tubes," Materials (Basel)., vol. 16, no. 1, p. 72, Dec. 2022, doi: 10.3390/ma16010072.

[25] "ECP 203-2018 (2018) Egyptian Code of Practise for Design of Reinforced Concrete Structures, fourth eddition, Egypt."

[26] "BS 8110–1. Structural use of concrete—Part 1: Code of practice for design and construction. London: British Standard Institution; 1997."

[27] "PrEN 1992–1-1:2020: Eurocode 2: Design of concrete structures – Part 1–1: General rules, rules for buildings, bridges and civil engineering structures. Final draft by the Project Team SC2.T1 working on Phase 1 of the CEN/TC 250 work programme under Mandat."

[28] "ACI-318–19, ACI Committee 318. Building Code Requirements for Structural Concrete (ACI 318- 19) and Commentary on Building Code Requirements (ACI 318–19). Farmington Hills (MI): American Concrete Institute; 2019."

[29] "Elstner, R. and Hognestad, E. (1956). 'Shearing strength of reinforced concrete slabs.' ACI Journal, Vol. 53, No. 1, pp. 29–58, DOI: 10.14359/11501."